

Structures of Ternary Complexes of BphK, a Bacterial Glutathione *S*-Transferase That Reductively Dechlorinates Polychlorinated Biphenyl Metabolites*

Received for publication, April 3, 2006, and in revised form, August 11, 2006. Published, JBC Papers in Press, August 17, 2006, DOI 10.1074/jbc.M603125200

Elitza I. Tocheva¹, Pascal D. Fortin², Lindsay D. Eltis, and Michael E. P. Murphy³

From the Department of Microbiology and Immunology, University of British Columbia, Vancouver, British Columbia V6T 1Z3, Canada

Prokaryotic glutathione *S*-transferases are as diverse as their eukaryotic counterparts but are much less well characterized. BphK from *Burkholderia xenovorans* LB400 consumes two GSH molecules to reductively dehalogenate chlorinated 2-hydroxy-6-oxo-6-phenyl-2,4-dienoates (HOPDAs), inhibitory polychlorinated biphenyl metabolites. Crystallographic structures of two ternary complexes of BphK were solved to a resolution of 2.1 Å. In the BphK-GSH-HOPDA complex, GSH and HOPDA molecules occupy the G- and H-sites, respectively. The thiol nucleophile of the GSH molecule is positioned for S_N2 attack at carbon 3 of the bound HOPDA. The respective sulfur atoms of conserved Cys-10 and the bound GSH are within 3.0 Å, consistent with product release and the formation of a mixed disulfide intermediate. In the BphK-(GSH)₂ complex, a GSH molecule occupies each of the two subsites. The three sulfur atoms of the two GSH molecules and Cys-10 are aligned suitably for a disulfide exchange reaction that would regenerate the resting enzyme and yield disulfide-linked GSH molecules. A second conserved residue, His-106, is adjacent to the thiols of Cys-10 and the GSH bound to the G-subsite and thus may stabilize a transition state in the disulfide exchange reaction. Overall, the structures support and elaborate a proposed dehalogenation mechanism for BphK and provide insight into the plasticity of the H-subsite.

Glutathione *S*-transferases (GSTs)⁴ transform a wide variety of electrophilic compounds in a reaction typically involving

* This work was supported by Discovery Grants from the Natural Sciences and Engineering Research Council (to L. D. E. and M. E. P. M.). The costs of publication of this article were defrayed in part by the payment of page charges. This article must therefore be hereby marked "advertisement" in accordance with 18 U.S.C. Section 1734 solely to indicate this fact.

The atomic coordinates and structure factors (code 2DSA and 2GDR) have been deposited in the Protein Data Bank, Research Collaboratory for Structural Bioinformatics, Rutgers University, New Brunswick, NJ (<http://www.rcsb.org/>).

□ The on-line version of this article (available at <http://www.jbc.org>) contains two supplemental figures.

¹ Recipient of a University Graduate Fellowship from the University of British Columbia.

² Recipient of Fonds pour la Formation de Chercheurs et l'Aide à la Recherche and Natural Sciences and Engineering Research Council postgraduate scholarships.

³ To whom correspondence should be addressed: Dept. of Microbiology and Immunology, Life Sciences Institute, University of British Columbia, 2350 Health Sciences Mall, Vancouver BC Canada V6T 1Z3. Tel.: 604-822-8022; Fax: 604-822-6041; E-mail: michael.murphy@ubc.ca.

⁴ The abbreviations used are: GST, glutathione *S*-transferase; PCB, polychlorinated biphenyls; HOPDA, 3-chloro-2-hydroxy-6-oxo-6-phenyl-2,4-dienoate; TCHQ, tetrachlorohydroquinone; MES, 2-morpholinoethanesulfonic acid; CDNB, 1-chloro-2,4-dinitrobenzene; GS, deprotonated GSH.

GSH (γ -L-Glu-L-Cys-Gly) conjugation (1). Best known for their roles in detoxification in eukaryotes, GSTs are also broadly distributed in prokaryotes as homo- or heterodimers with ~25-kDa subunits (2). To date, GSTs have been grouped into at least 12 distinct classes on the basis of substrate specificity and primary structure (3). The nomenclature is in flux due to the continued identification of new GSTs, particularly in prokaryotes (3, 4). Despite low sequence identity, all GSTs share a conserved two-domain structure (5) in which the N-terminal domain consists of a central core of a mixed four- or five-stranded β sheet buttressed by a pair of α helices, and the C-terminal domain is entirely α helical (1, 6, 7). The active site architecture is formed in part from two binding subsites located at the interface of two adjacent monomers. The G-subsite binds GSH, and the H-subsite binds hydrophobic electrophiles (8).

Most eukaryotic GSTs consume a single GSH that is conjugated to an electrophilic substrate during catalytic turnover (1). Bacterial GSTs function in a wide range of detoxification and catabolic pathways (9–11). Moreover, they display considerable diversity with respect to the utilization of GSH. For example, enzymes such as maleylacetoacetate and maleylpyruvate isomerases utilize but do not consume GSH (12). Interestingly, some bacterial GSTs, such as tetrachloro-hydroquinone (TCHQ) dehalogenase from *Sphingomonas chlorophenolica*, consume two GSH equivalents (13). The first GSH is used in the dehalogenation step leading to the formation of a mixed disulfide with the enzyme. The second equivalent of GSH is used to regenerate the free enzyme, yielding a disulfide-bridged product, GSSG. In a variation of this theme, the catabolism of lignin derivatives by *Sphingomonas paucimobilis* SYK-6 also consumes two GSH molecules but requires two enzymes to do so; LigF and LigG catalyze glutathione conjugations similar to eukaryotic enzymes and GSSG formation, respectively (14, 15). All of these GSTs are thought to involve GSH conjugation. However, their structural basis is poorly understood.

Insights obtained from the reported crystal structures of bacterial GSTs (8, 16) are limited as the second physiological substrates for these enzymes are unknown. The structure of PmGST B1-1 from *Proteus mirabilis* reveals the binding of GSH to the G-subsite with the thiol group covalently attached to Cys-10 (8). PmGST B1-1 binds antibiotics such as tetracyclines and rifamycin but at a site remote from the H-subsite (17). Similarly, the structure of an *Escherichia coli* GST was determined in a complex with the inhibitor glutathione sulfonate (*N*-(*N*- γ -L-glutamyl-3-sulfo-L-alanyl)-glycine) (16), a GSH ana-

Crystal Structures of BphK

logue. In this structure, Cys-10 and His-106 form hydrogen bonds to the glutathione sulfonate inhibitor; however, the bulky sulfonate group is unlikely to mimic a transition state (16). In many eukaryotic GSTs, Tyr-5 and Ser-11 are catalytically essential residues that are located in proximity to the sulfur atom of the bound GSH (8, 18). In the bacterial GSTs, these residues are not in contact with the bound GSH. Instead, two conserved residues, Cys-10 and His-106, interact directly with the GSH substrate and are ascribed catalytic roles (8). Site-directed mutagenesis studies using 1-chloro-2,4-dinitrobenzene (CDNB) as a reporter substrate failed to identify active site residues that activate the glutathione (19, 20).

The *bphK* gene of *Burkholderia xenovorans* LB400 encodes a GST that is part of the *bph* (biphenyl catabolic) pathway (21). The latter is responsible for the aerobic catabolism of biphenyl and the transformation of some polychlorinated biphenyls (PCBs). Biphenyl catabolism is typical of the aerobic catabolism of aromatic compounds in that it proceeds via a catechol, in this case 2,3-dihydroxybiphenyl (22). The extradiol cleavage of the latter produces 2-hydroxy-6-oxo-6-phenyl-2,4-dienoate (HOPDA), which is hydrolyzed to benzoate and 2-hydroxy-penta-2,4-dienoate in a reaction catalyzed by BphD. BphD is competitively inhibited by 3-Cl and 4-Cl HOPDAs (23). BphK is not essential for growth of *B. xenovorans* LB400 on biphenyl (24); however, BphK was shown recently to dechlorinate 3-Cl and 5-Cl HOPDAs (25). This activity would alleviate inhibition of the *bph* pathway by these PCB metabolites and likely contributes to the potent PCB-degrading ability of *B. xenovorans* LB400 (25). The reductive dehalogenation catalyzed by BphK is similar to that of TCHQ dehalogenase from *S. chlorophenolica* (26) in that it consumes two GSH equivalents (13). The BphK-catalyzed dehalogenation of 3-Cl HOPDA is proposed to proceed via either a simple addition of GSH followed by elimination of chloride or an S_N2 -mediated displacement (25). The second equivalent of GSH is used to regenerate the free enzyme.

To investigate the unusual catalytic mechanism of BphK and to probe the structural basis for catalysis in bacterial GSTs, we have obtained structural data for two ternary complexes of this enzyme. Each structure provides unique insights into the catalytic cycle of GSTs. In one structure, a HOPDA molecule (the dechlorinated product of 3-Cl HOPDA) and a GSH molecule are bound at the active site (BphK-GSH-HOPDA). In the other structure, two GSH molecules are bound at the active site of the enzyme (BphK-(GSH)₂). These structures support and extend the recently proposed mechanism (25). Furthermore, the structures reveal surprising flexibility of the active site to accommodate both HOPDA and GSH molecules at the H-subsite.

EXPERIMENTAL PROCEDURES

BphK was heterologously expressed in *E. coli* GJ1158 and purified using glutathione-Sepharose 4B resin as described previously (25). The stock BphK solution used in crystallization experiments contained 65 mg/ml of protein, 50 mM Tris, pH 8, and 10 mM GSH. The reservoir solution was 0.8–1.2 M K⁺/Na⁺ tartrate, 0.1 M MES, pH 6. BphK was crystallized by hanging drop vapor diffusion using a 1:1 ratio of reservoir to protein, and crystals grew within a week.

TABLE 1

Data collection and refinement statistics

Data were collected at 100 K.

	BphK-GSH-HOPDA	BphK-(GSH) ₂
Data collection		
Resolution (Å) ^a	50-2.1 (2.1–2.18)	50-2.1 (2.1–2.18)
Space group	R3	P6 ₅
Unit cell dimensions (Å)	$a = b = 112.2$, $c = 221.9$	$a = b = 103.4$, $c = 262.3$
Unique reflections	54562	87800
Completeness (%)	94.6 (88.8) ^a	97.0 (95.4)
Average I/σI	21.4 (1.6)	24.5 (6.2)
Redundancy	4.5 (2.9)	4.6 (3.4)
R_{merge}^b	0.058 (0.54)	0.061 (0.38)
Refinement		
$R_{\text{work}}/R_{\text{free}}$	0.204/0.236	0.161/0.204
Average B-values (Å ²)		
Overall	42.7	32.1
Protein	42.9	32.1
Ligands	41.4	33.0
Solvent	39.4	29.6
r.m.s. ^c deviations from ideality		
Bond lengths (Å)	0.010	0.012
Bond angles (degrees)	1.26	1.21

^a Numbers in parentheses correspond to those in the highest resolution shell.

^b $R_{\text{merge}} = \sum(|I - \langle I \rangle|) / \sum(I)$, where for each unique reflection, I is the observed intensity for each reflection merged, and $\langle I \rangle$ is the mean intensity.

^c r.m.s., root mean square.

Two co-crystallization experiments were performed: one with HOPDA and GSH and one with GSH alone. In the first experiment, the protein was diluted 1:1 with a buffer containing 2 mM HOPDA, 10 mM glutathione, and 50 mM Tris, pH 7. Before mounting, the crystals were soaked for an additional 30 min in 10 mM HOPDA, produced as described previously (23). In the second co-crystallization experiment, the protein was diluted 1:1 with a buffer containing 10 mM GSH and 50 mM Tris, pH 7. All crystals were transferred into mother liquor supplemented to 30% glycerol as a cryo-protectant.

The BphK-GSH-HOPDA co-crystals grew in space group R3 with unit cell dimensions $a = b = 112.2$ Å, $c = 221.9$ Å, and two dimers in the asymmetric unit (A-B, C-D). The BphK-(GSH)₂ co-crystals grew in space group P6₅ with unit cell dimensions $a = b = 103.4$ Å, $c = 282.3$ Å and three dimers (A-B, C-D, E-F) in the asymmetric unit. Data sets were collected at the Stanford Synchrotron Radiation Laboratory (SSRL) BL 9-1 to 2.1 Å resolution. The data were processed with DENZO and scaled with SCALEPACK (27). The overall Wilson B-factors were 42 and 30 Å² for the BphK-GSH-HOPDA and BphK-(GSH)₂ structures, respectively. The structure of a bacterial GST from *S. paucimobilis* (Protein Data Bank entry code 1F2E) with all non-conserved residues set to alanines was used as a starting model for molecular replacement using the program AMoRe with data to 2.8 Å resolution (28). The two proteins share 54% amino acid sequence identity, and the correlation coefficient and R-factor of the top solution were 0.59 and 0.53, respectively. Data collection and refinement statistics are presented in Table 1.

The BphK-GSH-HOPDA structure was refined using Refmac5 (29). Five percent of the data were set aside to calculate the free R-factor (30). Models were built and visualized using the program O (31). Electron density was observed at each of the four G-subsites, and GSH molecules were modeled at full occupancy. Electron density for the HOPDA molecule was present in all monomers and when modeled at half-

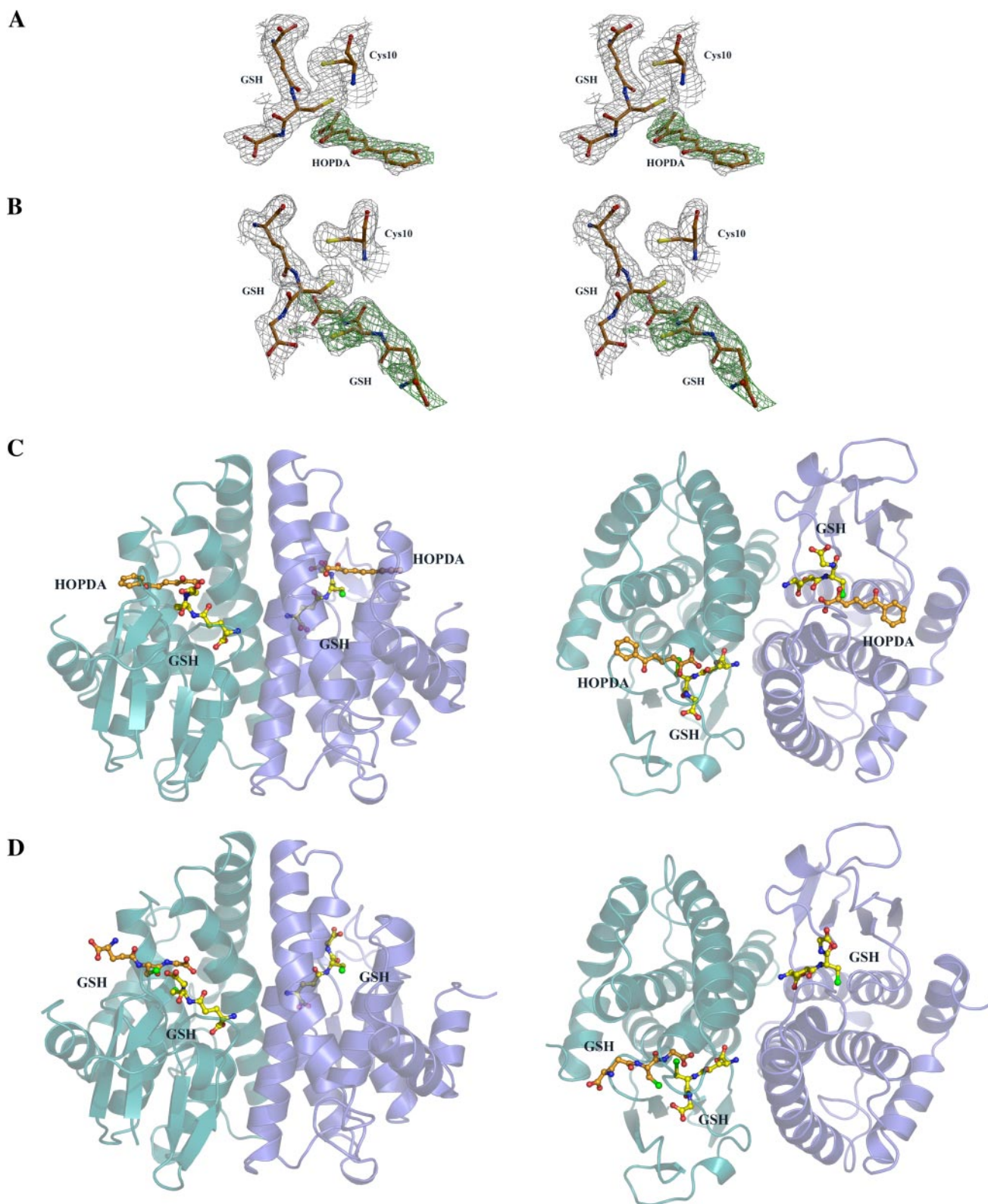


FIGURE 1. Crystal structures of BphK ternary complexes. *A*, stereo image of the bound ligands at the active site of the BphK-GSH-HOPDA complex. Residue Cys-10, GSH, and HOPDA molecules are shown as ball-and-stick models. $2F_o - F_c$ (gray) and omit $F_o - F_c$ (green) electron density maps are contoured at 0.9 and 2.9 σ , respectively. *B*, in the active site of the BphK-(GSH)₂ complex, the $2F_o - F_c$ electron density map (gray) is contoured at 0.9 σ . An omit $F_o - F_c$ electron density map of the GSH molecule at the H-subsite is shown in green and contoured at 2.5 σ . In panels *A* and *B*, carbon atoms are colored orange, nitrogen atoms are colored blue, oxygen atoms are colored red, and sulfur atoms are colored yellow. Ribbon diagrams of the BphK-GSH-HOPDA and BphK-(GSH)₂ homodimers are in panels *C* and *D*, respectively. The two monomers forming a functional dimer along (left) and perpendicular to (right) the local 2-fold axis are colored in slate and cyan. GSH and HOPDA molecules are shown as ball-and-stick models. Carbon atoms of the molecule bound to the G-subsite and the H-subsite are colored yellow and orange, respectively. Oxygen, nitrogen and sulfur atoms are colored red, blue, and green, respectively. Figs. 1 and 2 were generated using the programs Bobscript (40), Molscript (41), Raster3D (42), and PyMOL (43).

Crystal Structures of BphK

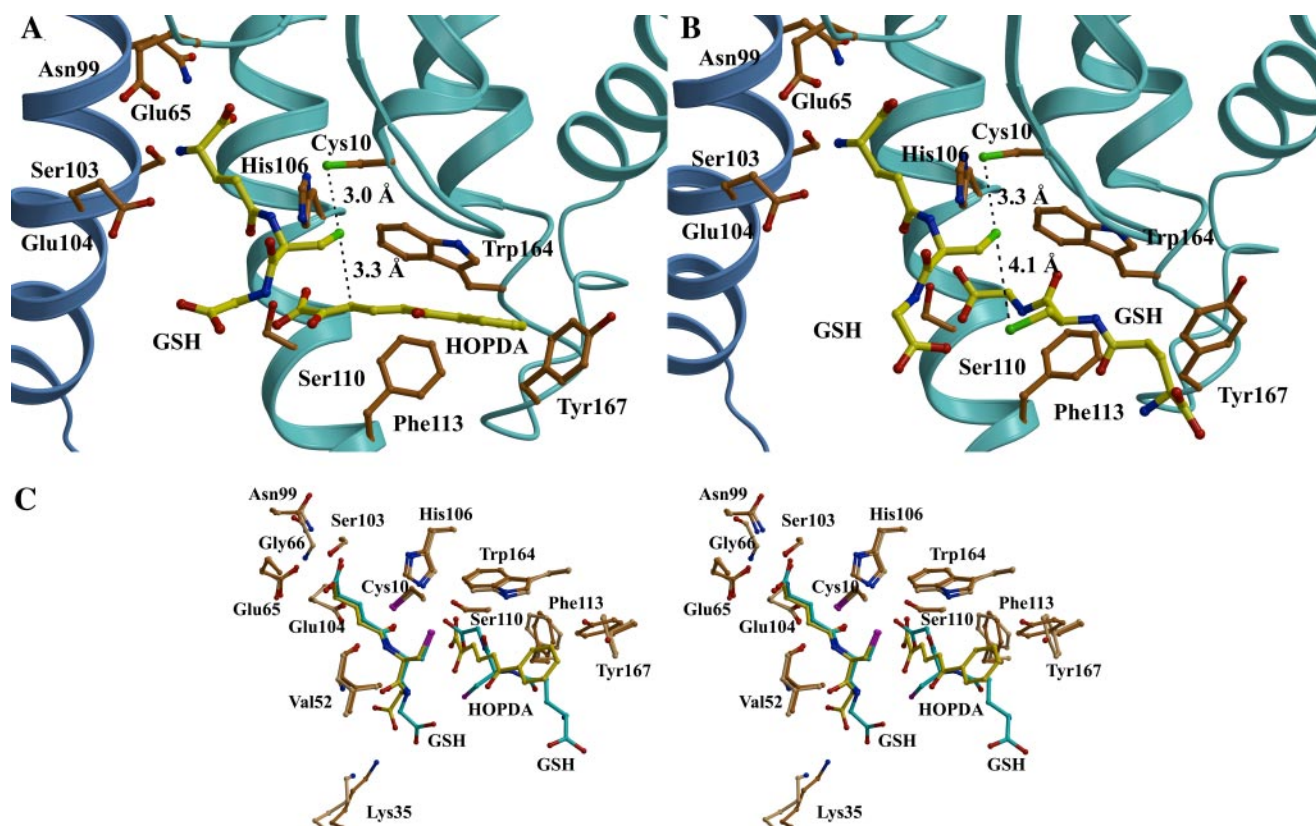


FIGURE 2. **The active sites of the BphK-GSH-HOPDA ternary complex (A) and the BphK-(GSH)₂ ternary complex (B).** Residues comprising the active site, the bound HOPDA, and the GSH molecules are shown as ball-and-stick models. Carbon atoms are colored yellow (GSH and HOPDA) and orange (amino acid side chains), nitrogen atoms are colored blue, oxygen atoms are colored red, and sulfur atoms are colored green. Secondary structures of the two monomers comprising a homodimer are colored in cyan and slate. Average distances are indicated beside dotted lines. C, stereo image of the superposition of the active sites of the BphK-GSH-HOPDA and the BphK-(GSH)₂ complexes. Side chain carbon atoms from the BphK-GSH-HOPDA complex are colored beige, and the GSH and HOPDA carbon atoms are colored yellow. Side chain carbon atoms from the BphK-(GSH)₂ complex are colored orange, and the carbon atoms of the two GSH molecules are colored cyan. In both structures, oxygen atoms are colored red, nitrogen atoms are colored blue, and sulfur atoms are colored magenta.

occupancy, refined with an average *B*-factor of 42 Å². The final model of the BphK-GSH-HOPDA complex contains four monomers, four GSH molecules, four HOPDA molecules, and 498 water molecules. The BphK-(GSH)₂ structure was refined using CNS (32). The crystal was almost perfectly twinned (33); the twin fraction for refinement and map calculations was refined to 0.45. Each of the six monomers contains one GSH substrate at the G-subsite. In three out of the six monomers, additional electron density was observed at the H-subsite and was modeled as a second GSH molecule. The occupancy of these second GSH molecules in monomers B, D, and F was set to 0.5, and the average *B*-factors were refined to 35 Å². The final model of the BphK-(GSH)₂ structure consists of six peptide chains, nine GSH molecules, and 216 water molecules. Ramachandran plots of the main chain torsional angles in each structure show that 95.0% of the residues are in the most favored regions, and none are observed in the disallowed regions as defined by PROCHECK (34).

RESULTS

The Overall Structure—The crystal structures of BphK-GSH-HOPDA and BphK-(GSH)₂ have two and three dimers in the asymmetric unit, respectively. The overall fold of BphK in the two structures is essentially identical (Fig. 1, C and D). The

root mean square deviation of the CA positions on superposition between each of the respective dimer pairs is less than 0.2 Å. Moreover, the main protein fold and subunit arrangement in the dimer are similar to those of other GSTs (1, 6, 7). Briefly, the monomer is comprised of two domains. The N-terminal domain (residues 1–79) contains a βαββ module (residues 1–38) connected to a βαα module (residues 54–77) via a long surface-exposed loop. A 12-residue linker connects the N-terminal domain to the C-terminal domain (residues 89–202). The latter domain contains five α helices. Each homodimer contains two equivalent active sites, which are found at clefts formed at the interface between the monomers (Fig. 1, C and D). A small portion of the active site cleft is formed by residues derived from the other monomer in the dimer (Fig. 2, A and B). The active site is comprised of two subsites, a common GSH binding site (G-subsite) and an H-subsite that typically binds the electrophilic second substrate of the reaction.

BphK-GSH-HOPDA Complex—Within the enzyme-GSH-product ternary complex, the GSH molecule is tightly held in an extended conformation at the G-subsite by 10 polar interactions (Fig. 2A, Table 2) and a single hydrophobic interaction with Tyr-51. The average *B*-factor of the atoms of the six GSH molecules is 41 Å², indicating that these sites are fully occupied

TABLE 2
Hydrogen bonds and distances

Interactions	Distances ^a	
	BphK-GSH-HOPDA	BphK-(GSH) ₂
Å		
BphK-BphK		
His-106 NE2–Cys-10 SG	4.17–4.30	3.83–3.93
His-106 ND1–Tyr-157 OH	2.73–2.83	2.57–2.65
BphK-G-subsite ligand		
His-106 NE2–GSH SG2	3.60–3.79	3.72–3.85
Cys-10 SG–GSH SG2	3.00–3.09	3.10–3.37
Glu-65 OE2–GSH N1	2.70–2.79	2.60–2.83
Ser-103 OG ^b –GSH N1	2.97–3.07	3.00–3.05
Asn-99 ND2 ^b –GSH O12	3.40–3.47	2.90–3.31
Gly-66 N–GSH O11	3.09–3.19	2.99–3.07
Glu-104 OE1 ^b –GSH N1	2.59–2.70	2.77–2.94
Lys-107 NZ–GSH OE1	3.66–3.91	3.38–3.43
Val-52 O–GSH N2	2.77–2.90	2.68–2.93
Val-52 N–GSH O2	2.78–2.87	2.89–3.19
Lys-35 NZ–GSH O31	2.96–4.80	2.64–2.98
BphK-H-subsite ligand		
His-106 NE2–GSH O31		3.27–3.44
Ser-110 OG–GSH O31		2.38–2.84
His-106 NE2–HPD ^c OA2	3.28–3.63	
Ser-110 OG–HPD OA1	2.66–3.19	
Ser-110 OG–HPD OA2	2.43–2.64	
Ligand-Ligand		
GSH SG2 _(G-subsite) –GSH SG2 _(H-subsite)		4.07–4.66
GSH SG _(G-subsite) –HPD CA3	3.16–3.41	

^a Range of distances over all the monomers in the asymmetric unit with both ligands bound.

^b Residues from adjacent subunit.

^c HPD, abbreviation for HOPDA molecule.

and that the bound molecules are well ordered. The glycyl moiety is orientated toward the surface of the protein, whereas the γ -glutamyl moiety is directed toward the core of the protein. The main interactions of the glycyl moiety are three hydrogen bonds involving Lys-35 and Val-52. The thiol of GSH forms a hydrogen bond with Cys-10 SG (3.0–3.1 Å) and is near to His-106 NE2 (3.6–3.8 Å). Three hydrogen bonds from the bound GSH are formed with residues from the adjacent monomer: Asn-99, Ser-103, and Glu-104. In addition, the γ -glutamyl moiety interacts with Glu-65 (a hydrogen bond) and Tyr-51 (hydrophobic interactions).

After refinement with GSH molecules bound at each of the four G-subsites and computing a difference map, strong electron density was observed in all of the monomers at the H-subsite adjacent to the modeled GSH. This density was fit and refined with a HOPDA molecule (Fig. 1A) in the *trans transoid* configuration of the enol tautomer, the predominant form in solution (23, 35). A HOPDA restraint library was created using the Monomer Library Sketcher within Refmac5. The enol tautomer is defined by CA2=CA3 and CA4=CA5 double bonds, whereas the keto tautomer is defined by a CA3=CA4 double bond (Fig. S2). When the keto form of the HOPDA molecule was modeled, the fit of the dienolate moiety was poor due to the disallowed rotation of the CA3=CA4 double bond.

When compared with the G-subsite, the H-subsite is more solvent-accessible, and BphK makes fewer direct interactions with the HOPDA product. Nonetheless, the HOPDA molecule refines with *B*-factors similar to those of the BphK atoms that form the H-subsite. The H-subsite is lined mainly with aromatic residues: Tyr-167, Phe-113, and Trp-164 (Fig. 2A). The base of this subsite is constructed from the peptide chain of

Gly-8 and Ala-9. Only three hydrogen bonds are formed with the HOPDA molecule, and all involve the carboxylate oxygen atoms. Two of these hydrogen bonds are with Ser-110 OG, and one is with His-106 NE2 (Table 2).

The single direct contact involving the two bound molecules in each subsite is a van der Waals interaction (~ 3.3 Å) between the GSH thiol and carbon 3 of the HOPDA molecule (Fig. 2A). Importantly, this carbon is chlorinated in the physiological substrate.

BphK:(GSH)₂ Complex—As in the BphK-GSH-HOPDA structure, the BphK-(GSH)₂ structure shows well defined electron density for a GSH molecule found in the G-subsite (Fig. 1B). The GSH molecule is in an extended conformation similar to the binding mode of the GSH molecule in the BphK-GSH-HOPDA structure. A shift of the glycyl moiety (corresponding to ~ 3.0 Å for the carboxylate oxygen atoms) is observed between the two structures (Fig. 2C). All the G-subsite protein-GSH interactions observed in the BphK-GSH-HOPDA structure are conserved in the BphK-(GSH)₂ structure (Table 2). An additional hydrogen bond is formed between Lys-107 NZ and OE1 of the GSH molecule bound at the G-subsite. More importantly, the position of the GSH sulfur atom with respect to Cys-10 SG and to His-106 NE2 is similar in the two structures (distances of 3.1–3.4 and 3.7–3.9 Å, respectively). When modeled in at full occupancy, the average *B*-factor of the GSH molecules was refined to 31 Å².

A second GSH molecule is observed at the H-subsite in three out of the six monomers (Figs. 1B and 2B). Although the second GSH was modeled at partial occupancy, clear density extends over the molecule, and the sulfur atom occupies the highest peak in an omit difference map (Fig. 1B). Similar to the binding of the HOPDA molecule, this second GSH molecule is sandwiched between the first GSH in the G-subsite and a hydrophobic pocket created by Tyr-167, Trp-164, and Phe-113. Only two hydrogen bonds are observed between the second GSH molecule and the protein. These interactions are between the glycyl carboxylate oxygen O31 of the GSH molecule and the residues His-106 and Ser-110 (Fig. 2B, Table 2).

This second GSH molecule is also bound in an extended conformation; however, the glycyl moiety is orientated toward Cys-10, and the γ -glutamyl moiety lies at the surface of the protein. As a result, the second GSH molecule is approximately antiparallel to the GSH molecule in the G-subsite such that the GSH sulfur atoms are 4.1–4.7 Å apart. Notably, His-106 NE2 serves as a bridge between the two GSH molecules by forming hydrogen bonds to the SG2 atom of GSH in G-subsite and O31 of GSH bound at the H-subsite (Table 2).

DISCUSSION

Structural Plasticity in the H-Subsite—BphK is typical of GSTs in that it binds a GSH molecule at its G-subsite and a second substrate at its H-subsite. Our crystal structures demonstrate the ability of the H-subsite of the enzyme to accommodate both a product and subsequently a second GSH molecule to accomplish the reductive dechlorination reaction. This flexibility seems to be linked to two properties of the H-subsite: a predominantly hydrophobic character and strategically positioned Ser and His residues. Thus, both ligands make hydro-

Crystal Structures of BphK

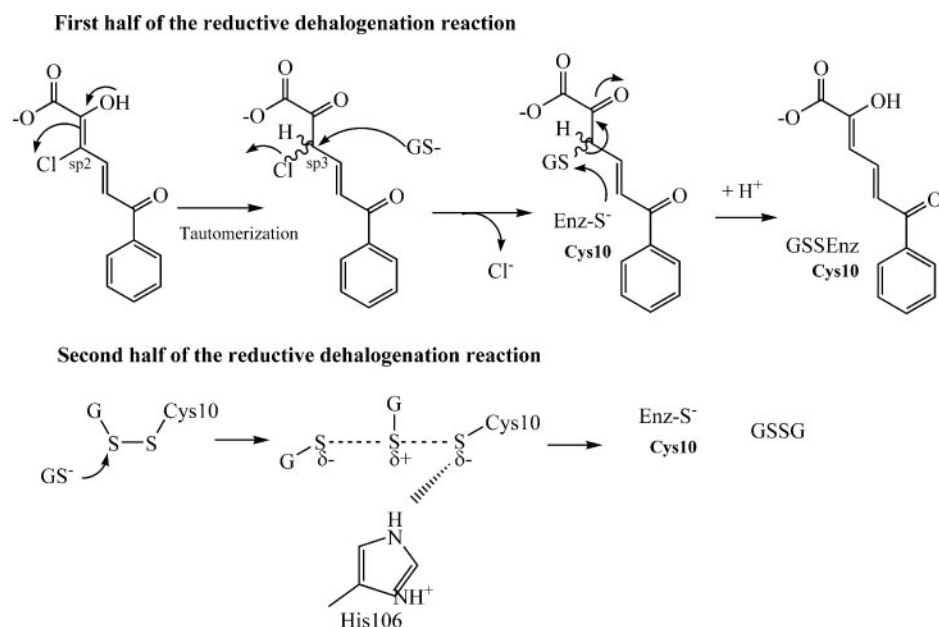


FIGURE 3. **Proposed mechanism for the BphK-catalyzed reductive dehalogenation of 3-Cl HOPDA.** The first half-reaction involves tautomerization of the HOPDA molecule followed by nucleophilic substitution to form a mixed disulfide. The second half-reaction is a disulfide exchange. Crystallographic data suggest that His-106 stabilizes the negative charge on Cys-10. *Enz*, enzyme.

phobic contacts with Trp-164, Tyr-167, and Phe-113 as well as hydrogen bonds to His-106 and Ser-110 (Fig. 2C). As discussed below, these interactions are important for orientating the compounds for productive catalysis. Differences in the configuration of the H-subsite residues involve Tyr-167 and Phe-113. To accommodate the HOPDA phenyl group in the BphK-GSH-HOPDA complex, the side chain of Tyr-167 rotates 80° about the χ_2 angle and the side chain of Phe-113 rotates 35° about the χ_2 angle. In addition, Tyr-167 is more ordered in the BphK-(GSH)₂ structure.

The relative paucity of specific interactions between the shallow and open H-subsite and each of the HOPDA and GSH molecules suggests that these ligands bind weakly. Indeed, these ligands were modeled at half-occupancy in the crystal structures despite being added in excess in the co-crystallization experiments. Consistent with these observations, BphK has a moderate specificity ($k_{\text{cat}}/K_m \sim 10^4 \text{ M}^{-1} \text{ s}^{-1}$) for 3-Cl HOPDA, suggesting that this enzyme is not highly adapted to its role in degrading PCBs (25). Weak binding is consistent with the broad substrate specificity typical of GSTs. For example, TCHQ dehalogenase binds the second GSH with a K_d value of 19 mM (36). In addition, the TCHQ substrate inhibited the formation of GSSG, suggesting that the aromatic substrate has higher affinity for the H-subsite (36). Thus, the observation of HOPDA binding to BphK in the presence of excess GSH is not surprising based on analogy between these enzymes.

Dehalogenation Reaction—Fortin *et al.* (25) proposed a mechanism for the BphK-catalyzed dehalogenation of 3-Cl and 5-Cl HOPDAs. This mechanism is similar to the better supported mechanism of TCHQ dehalogenase (26, 36) and can be divided into two half-reactions demarcated by the formation of a mixed disulfide between the enzyme and GSH. The first half-reaction was proposed to proceed via one of two routes: the

addition of GS^- at carbon 3 of HOPDA followed by elimination of Cl^- or the tautomerization of the enol(ate) followed by an $\text{S}_{\text{N}}2$ nucleophilic attack by GS^- at carbon 3 to release Cl^- . Either mechanism gives rise to a GS-HOPDA adduct from which the dehalogenated HOPDA molecule is released by nucleophilic attack of Cys-10 SG on the sulfur of the GS^- moiety, yielding a mixed disulfide linkage. In the second half-reaction, regeneration of the resting enzyme is initiated by the binding of a second GSH at the H-subsite for a final disulfide exchange. The result is a reduced sulfhydryl at Cys-10 and the formation of GSSG that leaves the active site (Fig. 3).

The binding mode and conformation of the GSH and HOPDA molecules at the H-subsite provides additional insights into the proposed mechanism. Although the dechlorination product is bound in the BphK-GSH-HOPDA complex, this structure is likely analogous to that for the binding of the 3-Cl substrate. Accordingly, a 3-Cl substituent would be orientated toward the indole ring of Trp-164. The nearest atom of the HOPDA molecule to the GSH thiol is carbon 3 (3.2–3.4 Å). Furthermore, the Burgi-Dunitz angle ($\sim 95^\circ$) is reasonable but not optimal (109°) for a nucleophilic substitution to proceed on an sp^2 carbon 3 (37). Carbon 5 is more distant from the nucleophile (~ 4.6 Å), but the enzyme readily dechlorinates 5-Cl HOPDA (25). Variation in the proposed mechanism or an alternate substrate binding mode may provide an explanation for the difference in catalytic activity on substrates chlorinated at different sites.

Of the two mechanisms proposed for the first half of the reductive dehalogenation reaction (25), the structural data are most consistent with those involving tautomerization and nucleophilic substitution (Fig. 3). In particular, the addition-elimination mechanism involves attack of GS^- on the sp^2 hybridized carbon 3 to form a tetrahedral intermediate resulting in the generation of a second negative charge on the carboxyl end of the HOPDA molecule. However, the structural data indicate that only Ser-110 coordinates to the HOPDA carboxylate and that this residue would poorly stabilize two negative charges on the carboxylate (Figs. 2A and 3). By contrast, the tautomerization-substitution mechanism eliminates the need for compensating groups to stabilize the additional negative charge on the carboxylate. Inspection of the H-subsite reveals no residue that could easily serve as a proton donor to catalyze the initial tautomerization. However, an intriguing possibility is that the HOPDA molecule is bound as the enol and that the 2-hydroxyl is the source of the proton at carbon 3. The $\text{p}K_a$ of 3-Cl HOPDA in solution is 6.1 (24) but may be perturbed by binding to the enzyme. Finally, the proposed mechanism for the first half-reaction of BphK differs from that of TCHQ dehalo-

genase, which involves chloride elimination from the aromatic ring followed by GSH attack (36).

The BphK-(GSH)₂ structure gives insight into the second half-reaction to regenerate the resting enzyme. In this structure, the distances between the sulfhydryls of Cys-10 and the two bound GSH molecules (>3.3 Å) indicate that all three sulfurs are reduced (Fig. 2B). Nonetheless, the sulfur atoms are aligned such that a disulfide could be formed easily either between Cys-10 and the GSH molecule (at the G-subsite) or between the two GSH molecules by small rotations of the χ_1 angles. His-106 is positioned to stabilize the anticipated development of a negative charge on Cys-10 that would result from a disulfide exchange reaction.

Comparison with Other β -GSTs—The overall fold of BphK is similar (CA root mean square deviation of <1.5 Å) to those of *E. coli* GST (16), PmGST B1-1 from *P. mirabilis* (8), and GST from *S. paucimobilis* (reported in Protein Data Bank entry 1F2E). Recently, site-directed mutagenesis studies on conserved structural motifs between residues Phe-151 and Ala-156 have identified their importance in protein folding and stability (38, 39). Conservation of structure is greater in the G-subsite, and the binding mode of a GSH molecule in this subsite of BphK is similar to that of PmGST B1-1 (8) and to the glutathione sulfonate analogue bound to the *E. coli* GST structure (16). A multiple sequence alignment (Fig. S1) reveals that BphK residues involved in the formation of the G-subsite are highly conserved among bacterial GSTs sharing at least 40% amino acid sequence identity. Residues Cys-10, Val-52, Glu-65, His-106, and Tyr-157 are absolutely conserved. Conservative substitutions are observed for Asn-99, Ser-103, and Glu-104. Position 51 has significant variability in the alignment and results in the greatest difference in the G-subsites between the BphK and the PmGST B1-1 structures. In PmGST B1-1, Gln-51 forms a weak hydrogen bond (3.6 Å) to the GSH, whereas in BphK, a Tyr at the equivalent position forms a hydrophobic interaction. A subtle difference between the two G-subsites is the distance between NZ of Lys-107 and OE1 of GSH. In the BphK-GSH-HOPDA complex, this distance is 3.7–3.9 Å, whereas in the PmGST B1-1 structure, that same interaction is a hydrogen bond (3.3 Å). Interestingly, this hydrogen bond is conserved in the BphK-(GSH)₂ structure (3.4 Å).

The hydrophobic character of the H-subsite in BphK is also conserved among bacterial GST sequences. Three conserved small residues (Pro-7, Gly-8, Ala-9) form one side of this subsite, and two conserved large hydrophobic residues (Phe-113, Trp-164) form the other side. Tyr-167 varies substantially and is substituted by histidine, arginine, or alanine in other bacterial GSTs. The identity of the residue at position 110 does not vary quite as much, being serine, glycine, valine, or threonine. The ternary complexes reported here suggest that Ser-110 and His-106 are important in defining H-subsite substrate specificity. The naturally observed substitutions at position 110 allow for variation in substrate specificity without sterically precluding the binding of a second GSH molecule.

In PmGST B1-1 and the GST from *S. paucimobilis*, a disulfide bridge is formed between the Cys-10 sulfur atom and SG2 of the GSH (8). The formation of this mixed disulfide provides a precedent for the intermediate formed at the end of the first half-reaction in the BphK dehalogenation mechanism (Fig. 3).

Cys-10 SG and His-106 have been hypothesized to activate GSH for the initial nucleophilic attack in related systems (8, 16); however, in our structures with reduced GSH in the active site, the hydrogen bonds to the GSH sulfur atom are weak, suggesting that little activation is necessary. Mutation of Cys-10 to Ser or Ala of PmGST B1-1 did not significantly reduce activity toward CDNB, a synthetic reporter substrate (19). Furthermore, the conservative mutation of His-106 to Asn had a greater impact on substrate binding than on catalysis using the same reporter substrate (20). Finally, mutational analysis of Ser, Tyr, and Thr residues in the active site failed to identify catalytically essential groups for GSH activation toward CDNB (19).

The reaction of some bacterial β -GSTs with CDNB is likely analogous to that observed in the larger GST superfamily, whereby a single GSH molecule is consumed and transferred giving a conjugated product (5). In contrast, the mechanism for BphK is a reductive dehalogenation requiring two GSH equivalents; the transferase reaction constitutes only a part of the first half-reaction. Thus, use of CDNB as a reporter substrate provides information only for the first two steps of a more complex mechanism (Fig. 3). Interestingly, mutation of an active site Cys in TCHQ dehalogenase does not prevent the initial GSH nucleophilic attack on substrate but does reduce overall activity 10-fold (36). The proposed mechanism for BphK and the crystal structures presented here suggest that conserved active site residues are not critical for the initial GSH transferase reaction but facilitate the subsequent catalytic steps.

Mutational studies on BphK directed at Cys-10 and His-106 are not yet available; however, a conserved region from Ser-152 to Leu-158 was targeted in a recent study (39). In the crystal structure of BphK, the phenolic oxygen of Tyr-157 within this region forms a hydrogen bond to ND1 of His-106, which likely determines the orientation of the imidazole ring. An analysis of activity toward CDNB and 4-chlorobenzoate, a proposed alternative physiological substrate for BphK, showed that this region is not directly involved in substrate recognition and catalysis (39). The chlorinated HOPDAs are 1000-fold better substrates than 4-chlorobenzoate (25), and the reaction for the latter is likely to be analogous to that of CDNB. Further evaluation of the role of Cys-10 and His-106 awaits studies using chlorinated HOPDA substrates or appropriate analogues. Conservation of these residues in the β -GSTs suggests that a reductive mechanism involving the consumption of two GSH molecules may be a general feature of this bacterial class.

Acknowledgments—Portions of this research were carried out at the Stanford Synchrotron Radiation Laboratory, a national user facility operated by Stanford University on behalf of the U.S. Department of Energy, Office of Basic Energy Sciences. The SSRL Structural Molecular Biology Program is supported by the Department of Energy, Office of Biological and Environmental Research, and by the National Institutes of Health, National Center for Research Resources, Biomedical Technology Program. We thank Geoff Horsman for stimulating discussions, Cheryl Whiting for protein purification, and Christine Florizone for product synthesis.

REFERENCES

1. Armstrong, R. N. (1997) *Chem. Res. Toxicol.* **10**, 2–18
2. Mannervik, B., and Danielson, U. H. (1988) *CRC Crit. Rev. Biochem.* **23**, 283–337
3. Vuilleumier, S., and Pagni, M. (2002) *Appl. Microbiol. Biotechnol.* **58**, 138–146
4. Oakley, A. J. (2005) *Curr. Opin. Struct. Biol.* 716–723
5. Vuilleumier, S. (1997) *J. Bacteriol.* **179**, 1431–1441
6. Dirr, H., Reinemer, P., and Huber, R. (1994) *Eur. J. Biochem.* **220**, 645–661
7. Wilce, M. C., and Parker, M. W. (1994) *Biochim. Biophys. Acta* **1205**, 1–18
8. Rossjohn, J., Polekhina, G., Feil, S. C., Allocati, N., Masulli, M., De Ilio, C., and Parker, M. W. (1998) *Structure (Lond.)* **6**, 721–734
9. Di Ilio, C., Aceto, A., Piccolomini, R., Allocati, N., Faraone, A., Cellini, L., Ravagnan, G., and Federici, G. (1988) *Biochem. J.* **255**, 971–975
10. Iizuka, M., Inoue, Y., Murata, K., and Kimura, A. (1989) *J. Bacteriol.* **171**, 6039–6042
11. Arca, P., Garcia, P., Hardisson, C., and Suarez, J. E. (1990) *FEBS Lett.* **263**, 77–79
12. Polekhina, G., Board, P. G., Blackburn, A. C., and Parker, M. W. (2001) *Biochem. J.* **40**, 1567–1576
13. Anandarajah, K., Kiefer, P. M., Jr., Donohoe, B. S., and Copley, S. D. (2000) *Biochemistry* **39**, 5303–5311
14. Masai, E., Katayama, Y., Nishikawa, S., and Fukuda, M. (1999) *J. Ind. Microbiol. Biotechnol.* **23**, 364–373
15. Masai, E., Ichimura, A., Sato, Y., Miyauchi, K., Katayama, Y., and Fukuda, M. (2003) *J. Bacteriol.* **185**, 1768–1775
16. Nishida, M., Harada, S., Noguchi, S., Satow, Y., Inoue, H., and Takahashi, K. (1998) *J. Mol. Biol.* **281**, 135–147
17. Perito, B., Allocati, N., Casalone, E., Masulli, M., Dragani, B., Polsinelli, M., Aceto, A., and Di Ilio, C. (1996) *Biochem. J.* **318**, 157–162
18. Sheehan, D., Meade, G., Foley, V. M., and Dowd, C. A. (2001) *Biochem. J.* **360**, 1–16
19. Casalone, E., Allocati, N., Ceccarelli, I., Masulli, M., Rossjohn, J., Parker, M. W., and Di Ilio, C. (1998) *FEBS Lett.* **423**, 122–124
20. Allocati, N., Casalone, E., Masulli, M., Polekhina, G., Rossjohn, J., Parker, M. W., and Di Ilio, C. (2000) *Biochem. J.* **351**, 341–346
21. Hofer, B., Backhaus, S., and Timmis, K. N. (1994) *Gene (Amst.)* **144**, 9–16
22. Furukawa, K. (2000) *J. Gen. Appl. Microbiol.* **46**, 283–296
23. Seah, S. Y. K., Labbe, G., Nerdinger, S., Johnson, M. R., Snieckus, V., and Eltis, L. D. (2000) *J. Biol. Chem.* **275**, 15701–15708
24. Bartels, F., Backhaus, S., Moore, E. R. B., Timmis, K. N., and Hofer, B. (1999) *Microbiology (Read.)* **145**, 2821–2834
25. Fortin, P. D., Horsman, G. P., Yang, H. M., and Eltis, L. D. (2006) *J. Bacteriol.* **188**, 4424–4430
26. Kiefer, P. M., Jr., and Copley, S. D. (2002) *Biochemistry* **41**, 1315–1322
27. Otwinowski, Z., and Minor, W. (1997) *Methods Enzymol.* **276**, 307–326
28. Collaborative Computational Project, N. (1994) *Acta Crystallogr. Sect. D Biol. Crystallogr.* **50**, 760–763
29. Murshudov, G. N., Vagin, A. A., and Dodson, E. J. (1997) *Acta Crystallogr.* **53**, 240–255
30. Brünger, A. T. (1992) *Nature* **355**, 472–475
31. Jones, T. A., Zou, J.-Y., Cowan, S. W., and Kjeldgaard, M. (1991) *Acta Crystallogr. Sect. A* **47**, 110–119
32. Brunger, A. T., Adams, P. D., Clore, G. M., Delano, W. L., Gros, P., Grosse-Kunstleve, R. W., Jiang, J. S., Kuszewski, J., Nilges, N., Pannu, N. S., Rice, L. M., Simonson, T., and Warren, G. L. (1998) *Acta Crystallogr. Sect. D Biol. Crystallogr.* **54**, 905–921
33. Yeates, T. O. (1997) *Methods Enzymol.* **276**, 344–358
34. Laskowski, R. A., Moss, D. S., and Thornton, J. M. (1993) *J. Mol. Biol.* **231**, 1049–1067
35. Catelani, D., and Colombi, A. (1974) *Biochem. J.* **143**, 431–434
36. Warner, J. R., Lawson, S. L., and Copley, S. D. (2005) *Biochemistry* **44**, 10360–10368
37. Burgi, H. B., Dunitz, J. D., Lehn, J. M., and Wipff, G. (1974) *Tetrahedron* **30**, 1563
38. Allocati, N., Masulli, M., Pietracupa, M., Federici, G., and Di Ilio, C. (2006) *Biochem. J.* **394**, 11–17
39. Gilmartin, N., Ryan, D., and Dowling, D. N. (2005) *FEMS Microbiol. Lett.* **249**, 23–30
40. Esnouf, R. M. (1999) *Acta Crystallogr. Sect. D Biol. Crystallogr.* **55**, 938–940
41. Kraulis, P. (1991) *J. Appl. Crystallogr.* **24**, 946–950
42. Merritt, E. A., and Bacon, D. J. (1997) *Methods Enzymol.* **277**, 505–524
43. Delano, W. L. (2002) *The PyMOL Molecular Graphics System*, DeLano Scientific, San Carlos, CA
44. Thompson, J. D., Gibson, T. J., Plewniak, F., Jeanmougin, F., and Higgins, D. G. (1997) *Nucleic Acids Res.* **25**, 4876–4882
45. Hall, T. A. (1999) *Nucleic Acids Symp. Ser.* **41**, 95–98

SUPPLEMENTAL DATA

FIG. S1. Multiple sequence alignment of bacterial GSTs. The accession numbers of the sequences used are as follows: BphK_LB400 (GST from *Burkholderia xenovorans* LB400, CAD44474.1), GST_Pmi (GST from *Proteus mirabilis*, AAC44362.1), GST_Eco (GST from *Escherichia coli*, ZP_00926596.1), GST_Spa (GST from *Sphingomonas paucimobilis*, AAC46031.1), GST_Rfe_15236 (GST from *Rhodoferrax ferrireducens*, ZP_00695363), GST_Pna (GST from *Polaromonas naphthalenivorans* CJ2, ZP_01019796.1), GST_Rpa (GST from *Rhodopseudomonas palustris*, NP_946173.1), GST_Ype (GST from *Yersinia pestis*, NP_405903.1). Black shading indicates absolutely conserved residues and grey shading indicates conservative amino acid substitutions. Red and black asterisks indicate residues forming the G-subsite and H-subsite, respectively. The alignment was generated using ClustalX (44) and formatted with BioEdit (45).

FIG. S2. Ball-and-stick representation of the HOPDA product with all atoms labeled.

FIG. S1

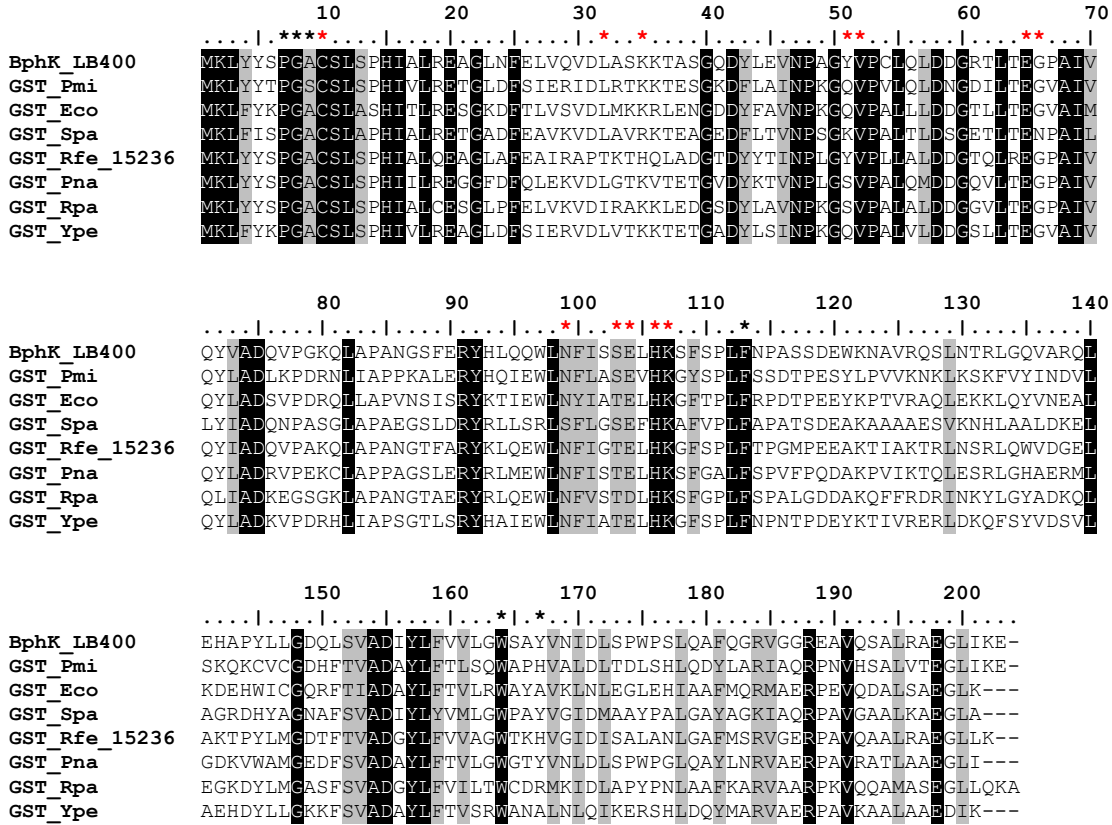
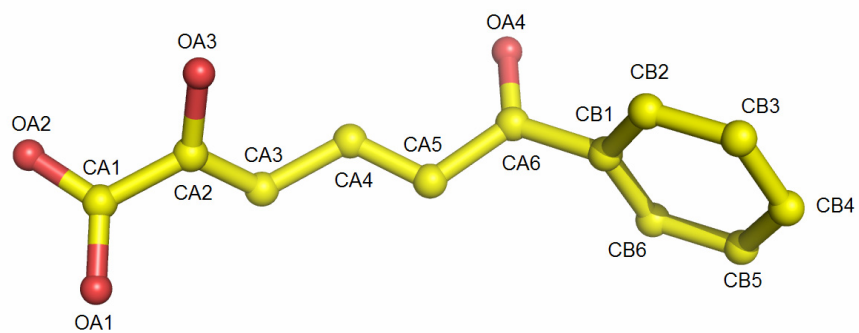


FIG. S2



Structures of Ternary Complexes of BphK, a Bacterial Glutathione S-Transferase That Reductively Dechlorinates Polychlorinated Biphenyl Metabolites

Elitza I. Tocheva, Pascal D. Fortin, Lindsay D. Eltis and Michael E. P. Murphy

J. Biol. Chem. 2006, 281:30933-30940.

doi: 10.1074/jbc.M603125200 originally published online August 17, 2006

Access the most updated version of this article at doi: [10.1074/jbc.M603125200](https://doi.org/10.1074/jbc.M603125200)

Alerts:

- [When this article is cited](#)
- [When a correction for this article is posted](#)

[Click here](#) to choose from all of JBC's e-mail alerts

Supplemental material:

<http://www.jbc.org/content/suppl/2006/08/18/M603125200.DC1>

This article cites 43 references, 11 of which can be accessed free at

<http://www.jbc.org/content/281/41/30933.full.html#ref-list-1>